Controllable wavelength conversion based on soliton dynamics in mid-infrared fiber

Kangle Shen[1], Jian Yang[2], Jiayi Zhao[1], Xinyu Yang[1], Hua Yang[1,3,*]

[1]College of Computer Science and Electronic Engineering,
 Key Laboratory for Micro/Nato Optoelectronic Devices of Ministry of Education,
 Hunan University, Changsha 410082, China

[2]Hunan University of Chinese Medicine, Changsha 410082, China

[3]State Key Laboratory of Integrated Optoelectronics, Institute of Semiconductors,
 Chinese Academy of Sciences, Beijing 10008, China

*Corresponding author: huayang@hnu.edu.cn

We provide a convenient way to actively control the wavelength conversion of probe waves based on the soliton dynamics in the As_2S_3 fibers. In this paper, it is found by numerical calculation that wavelength conversion occurs in the frequency domain due to the existence of refractive index barrier. By adjusting the collision position of pump pulse and probe pulse to realize the conversion of probe pulse wavelength, the effect of the power and the incident wavelength of the probe wave on the wavelength conversion are also discussed. This frequency domain conversion is of great use in the mid-infrared region, for example, all-optical conversion switches.

Keywords: soliton dynamics, photonic crystal fiber, all-optical conversion switches.

1. Introduction

Due to the high nonlinearity, low confinement loss and tunable chromatic dispersion of the photonic crystal fibers (PCFs), ultrashort pulses dynamics in PCFs have been extensively studied both in experimental and theoretical [1]. It plays an important role in technological applications in photonics, like the formation of solitons, resonant radiation, supercontinuum generation and interaction of solitons with dispersive waves (DW). The soliton–DW interaction has been the issue of fundamental study in this area [2,3]. Optical event horizon in optical fibers based on the dynamics of soliton–DW interaction is one of distinguished research [4] and it is useful in numerous fields such as light control [5-7]. It happens when pump pulse's group velocity is different from that of a probe both transmitting in a fiber. The pump pulse acts as a strong refractive index barrier, and the weak probe pulses will experience a wavelength conversion when reflected on the barrier [5,8,9].

The nonlinear mechanism behind the soliton–DW interaction is that soliton with high intensity changes the velocity of the weak probe pulses and contributes to the generation of new frequency which is conversed from weak probe pulses. The two-pulse collision based on optical pulse interaction mechanism in optical fibers can also be understood as a four-wave-mixing (FWM) process [10-13]. It has been pointed out as an efficient mechanism to convert the frequency of a signal [14] in a complementary manner from the interactions involving the emission of a Cherenkov radiation in an optical analogue.

At the same time, there is a significant research effort focused on extending the wavelength coverage toward the mid-Infrared (mid-IR) in the 2–20 μm molecular fingerprint region currently [15-20]. But the generation of these mid-infrared supercontinua requires a 2–5 μm ultrasoft pulse source, and the current methods of implementation are optical parametric oscillators (OPO) and amplifiers (OPA) [2]. They are typically expensive and cumbersome [4, 21, 22]. In this paper, based on the basic principles of soliton dynamics, we realize the upward and downward conversion of the probe pulse wavelength in the mid-infrared region, and the maximum conversion amplitude can reach 310 nm. Then we also explore the influence of the power and position of the probe pulse on the wavelength conversion. The frequency conversion on the arsenic sulfide fiber explored in this simulation experiment is carried out under the consideration of all nonlinear effects to ensure the accuracy of the experiment, which has a guiding role for future research on the control of light with light.

This paper is organized as follows. In Section 2, we study the theoretical model of a PCF with two pulses under the generalized nonlinear Schrödinger equation (GNLSE). In Section 3, we describe the generation of wavelength conversion with ultrashort pulses in time domain and frequency domain, respectively. In Section 4, by changing the position and energy of the probe pulse, the influence of the parameters on the output probe wave is discussed.

2. Theoretical model and fiber analysis

We use a As_2S_3 microstructured fiber here. It has one zero dispersion wavelength (λ_{ZDW} = 2203 nm). The fiber under investigation in our model has six-order dispersion parameters at 1550 nm: β_2 = 339.16 ps^2/km, β_3 = 0.721 ps^3/km, β_4 = –7.849 × 10^{-4} ps^4/km, β_5 = 2.5368 × 10^{-6} ps^5/km, and β_6 = –1.0391 × 10^{-8} ps^6/km. Figure 1 depicts the corresponding dispersion and group delay curves.

In the As_2S_3 optical fiber [18, 23-25], the nonlinear coefficient is a very important parameter, and it decreases with the increase of incident wavelength, so it is necessary to calculate the nonlinear coefficient of optical fiber corresponding to different pump wavelength. We can obtain the nonlinear coefficient corresponding to different pumping wavelength by $\gamma = (n_2 w_0)/(c A_{eff})$, where n_2 represents the nonlinear refractive index coefficient, w_0 represents the pulse center angular frequency, c represents the speed of light in a vacuum, and A_{eff} represents the effective core area. The nonlinear coeffi-
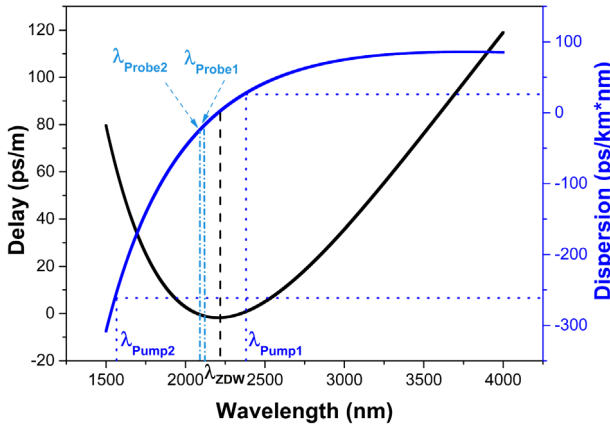
Fig. 1. The dispersion (blue curve) and group delay (black curve) profiles in terms of the pump wavelength in the As$_2$S$_3$ fiber. There is a zero dispersion point at 2203 nm.

cient is taken as $\gamma = 2150$ W^{-1}km^{-1} at 1550 nm. The computation of the refractive index is based on the Sellmeier equation [19].

Besides, the length of fiber is short and we neglected propagation loss here. The evolution of the complex envelope $A(z, t)$ of the electric field in an optical fiber can be described with the help of a generalized nonlinear Schrödinger equation (GNLSE) [1,17]:

$$\frac{\partial A}{\partial z} = -\frac{\alpha}{2} A + \sum_{k \geq 2} \frac{i^{k+1} \beta_k}{k!} \frac{\partial^k A}{\partial t^k}$$

$$+ i\gamma \left(1 + i\tau_{\text{sh}} \frac{\partial}{\partial t}\right) \left[A(z, t) \int_{-\infty}^{+\infty} R(t')|A(z, t-t')|^2 dt' \right] \tag{1}$$

The electric field envelope is $A(z, t)$, it presents the time conveying at the pulse group velocity β_1^{-1} and z is the transmission length. The linear loss coefficient is represented by α. β_k are the k-th-order dispersion coefficients in normalized form describing the linear dispersion effect. γ is the nonlinear coefficient. $\tau_{\text{sh}} = \omega_0^{-1}$ is related to the effects such as optical shock formation and self-steepening. Response function $R(\tau) = f_R h_R(\tau) + (1 - f_R)\delta(\tau)$ includes instantaneous electronic contribution and delayed Raman contribution [1,17], with $f_R = 0.17$ and $h_R(\tau) = \exp(-\tau/\tau_2)\sin(-\tau/\tau_1) \times$ $\times (\tau_1^2 + \tau_2^2)/(\tau_1 \times \tau_2^2)$. Here $\tau_1 = 15.5$ fs and $\tau_2 = 230.5$ fs are both delay times in the As$_2$S$_3$ optical fiber.

We excite the fiber using two pulses with different frequencies, named the pump pulse and the probe pulse, respectively. The input electric field of $A(0, t)$ is determined as the following form propagating in PCF.

$$A(z, t) = \sqrt{P_0} \exp\left(-\frac{t^2}{2T_0^2}\right) + a_0\sqrt{P_0} \exp(i\,2\pi f_{\mathrm{mod}}\,t)\exp\left(-\frac{(t + t_{\mathrm{del}})^2}{2T_0^2}\right) \quad (2)$$

Here $T_0 = \tau_0/1.665 = 50$ fs, it represents the half-width of the pulse. P_0 represents the normalized peak power of input pulse, and the normalized peak power of the probe is defined as $a_0^2 P_0$. We use a fundamental Gaussian pulse as the pump pulse and its peak power is 1.52 kW. In order to observe obvious experimental phenomena, $a_0 = 0.32$ is chosen at first. It means that the energy of the probe pulse is one-tenth that of the energy of the pump pulse. We first consider one pump propagating in anomalous dispersion regime, centred at an optical wavelength $\lambda_0 = 2350$ nm and accompanied by a weak probe which has a frequency offset (f_{mod}) and time delay (t_{del}) with respect to the pump pulse propagating in normal dispersion regime.

3. Soliton dynamics of wavelength conversion

To observe the formation of wavelength conversion, the initial conditions of injected pulses are adjusted suitably to interact with each other. When the group velocities of the two pulses are quite different, they will go through each other. On the contrary, if the pulses are set too close, they may never meet [12]. The two input pulses need to meet the wave-number matching curve. That is, an optical soliton (ω_s) propagating in the anomalous dispersion region collids with a weak probe wave (ω_p) in the normal dispersion region of the fiber. The probe wave undergoes a nonlinear frequency conversion into a pulse with a center frequency of ω_I. The center frequency of the pulse is determined by the oscillation conditions:

$$\hat{D}(\omega_p - \omega_s) = \hat{D}(\omega_I - \omega_s) \tag{3}$$

$$\hat{D}(\omega - \omega_s) = \sum_{k \geq 2} \frac{\beta_k}{k!}\left[\omega - \omega_s\right] \tag{4}$$

We inject the probe prior or posterior to the intense pump with a suitable delay through repeated testing, gradually increasing the pump power until the emergence of the probe pulse colliding with the pump pulse and generating a clear frequency conversion in the spectrum. Figure 2 shows the corresponding simulations.

As the time domain evolution shows, an interesting phenomenon arises when the pump pulse ($\lambda_{\mathrm{pump}} = 2350$ nm) and the probe ($\lambda_{\mathrm{probe}} = 2114$ nm) are propagating together down the fiber. The pump pulse has an obvious soliton self-frequency shift because it is located in the anomalous dispersion region [23]. The input pulse is initiated by the joint effect of self-phase modulation (SPM) and group velocity dispersion (GVD) at the initial stage of propagation. The fundamental soliton undergoes the Raman self-frequency shift under the effect of stimulated Raman scattering (SRS). With the in-
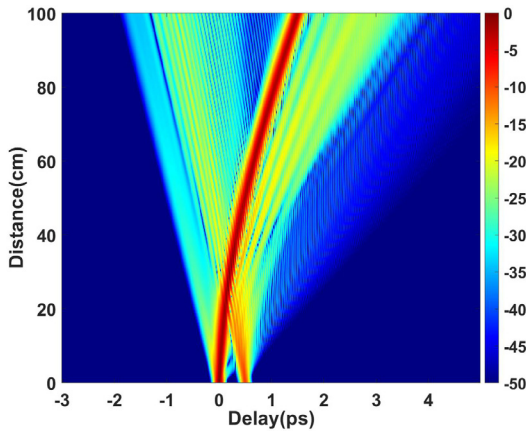
Fig. 2. Time-domain evolution of a solition pulse (λ_{pump} = 2350 nm) colliding with a delayed probe (λ_{probe} = 2114 nm), and the time of detection wave ahead of pump wave is 0.48 ps.

crease of the transmission distance, the fundamental soliton moves to long wavelength, accompanied by the decrease of group velocity. While the probe pulse is located in the normal dispersion region, it exists mainly in the form of dispersion waves in the arsenic sulfide fiber. At first, the pump pulse precedes the probe pulse. As shown in the figure, the rate of the probe pulse remains almost constant as it travels. At the same time, the velocity of soliton constantly decreases as constant red shift, to collide finally at 19.8 cm.

It is obvious from Fig. 2 that a nonlinear disturbance of the refractive index is produced when the probe reaches the pump pulse, preventing two pulses from crossing each other, which then leads to an obvious "reflection" barrier. Both velocities of them are slightly different as a result of the combination of normal dispersion and cross -phase modulation. It is worth noting that the probe pulse is substantially scattered and converts into new spectral components, only few parts of it transmit and follow the original trajectory. In fact, the soliton creates a moving refractive index perturbation that changes the velocity of the probe wave and prevents it from penetrating the soliton. The probe may even be caught entirely by the pump pulse in extreme cases. The scattering means a frequency conversion in the case of non-uniform motion, as is shown in Fig.3(a), which is always described as an optical event horizon and we observed this phenomenon for the first time in the mid-infrared region.

This variation can also be shown on a frequency domain diagram in Fig. 3(a), at the initial stage of propagation in the frequency domain, because the input pulse is a fundamental soliton pulse, so a distinct soliton is formed only in the time domain, which keeps its shape and keeps moving towards longer wavelength at smaller and smaller speeds. For the probe pulse, it undergoes a linearly broadening at first. Then at 19.8 cm, the pump pulse and probe collide, the motion track of the probe pulse changes visibly and experiences frequency conversion from 2114 to 1975 nm at the distance from 19.8 to 29.2 cm. With further propagation along the fiber, the new fre-
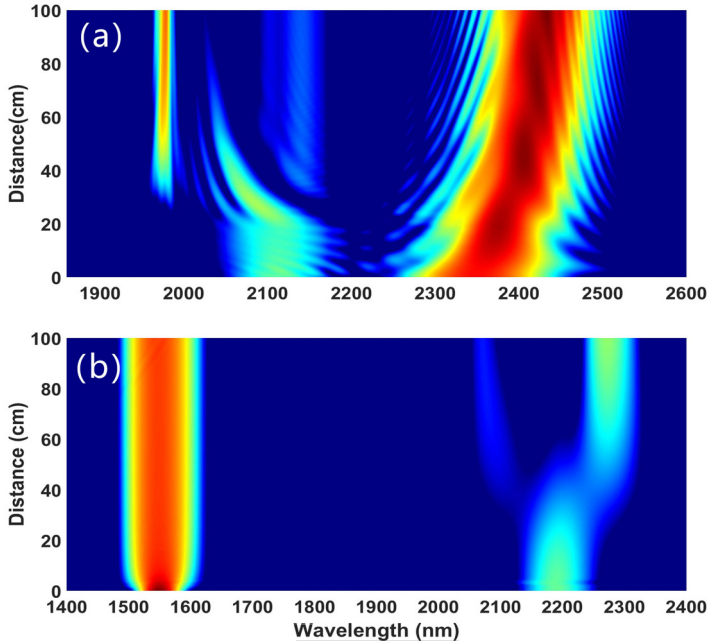
Fig. 3. Frequency-domain evolution (a) of a pump pulse (λ_{pump} = 2350 nm) colliding with probe pulse (λ_{probe} = 2114 nm), representing a typical wavelength down conversion. Frequency-domain evolution (b) of a pump pulse (λ_{pump} = 1550 nm) colliding with probe pulse (λ_{probe} = 2250 nm) under suitable delay conditions, representing a typical wavelength up conversion.

quency generates. By calculation, at the new frequency there is almost a Gaussian pulse, and the peak power is higher more than ten times than that before conversion. This is very important for us to use this characteristics for all-optical conversion.

Under the guidance of this principle, not only the probe pulse can be converted to short wavelength, but also to long wavelength. Now the pump pulse remains the same as the previous parameter but the wavelength of the pump pulse was changed to 1550 nm. In this case, the pump waves incident in the normal dispersion region, resulting in a sharp spectral broadening, producing a very flat super-continuum. As shown in Fig. 3, by adjusting the time delay appropriately, the probe wave and the pump wave collide at 29.8 cm. At the distance from 30 to 49.2 cm, the two pulses interact and a longer wavelength is created. It has been calculated that the energy transfer efficiency of the probe pulse in both cases is up to 97% with almost no energy loss. Moreover, the pulse shape after wavelength conversion still retains the original shape, which can reduce the post-processing of pulse waveform in practical application.

We can see this in Fig. 3, where the wavelength conversion to long wavelength is more obvious than that to the short wavelength direction, which is mainly limited by the group velocity matching. Also we can further extend the range of wavelength conversion to blue wavelength by changing the slope of the short wavelength side of the group dispersion curve through designing the cross-section structure of the fiber.

4. Result and discussion

4.1. The influence of probe pulse wavelength

In order to explore the wavelength conversion process more clearly, we explore the influence of initial pulse parameters on wavelength conversion. The probe pulse is tuned from 1980 to 2279 nm. The corresponding results are depicted in Fig. 4. In our experiment, the probe pulse wavelength is shorter than 1980 nm and is too far from the pump wave. Then the group velocities of the two groups are mismatched, unable to collide, and thus unable to produce short-wavelength conversion. Also when the probe pulse wavelength is longer than 2279 nm, the position of the pump wave almost coincides with that of the pump wave, and their interaction mechanism becomes very intense and complicated; we do not pay attention to that situation either.

As it is shown in Fig. 4, we can see that when the range of the probe wave is changed from 1980 to 2279 nm, the corresponding wavelength after transition is almost centered at about 1980 nm, and the wavelength fluctuation range is very small, thus there is an excellent consistency. But even more important is the fact that we can see that this wavelength conversion mechanism can compress the pulse width to get almost the same pulse as the probe pulse. As shown in Fig. 2, at the distance of 0.1 to 19.8 cm, after experiencing various nonlinear effects in the normal dispersion region, the probe pulse of 70 fs is widened tens of times. But high energy pulses of very narrow pulse width are generated at the distance of 35.2 cm, whose peak intensity was more than 20 times higher than that before the conversion. Taking advantage of this property of the probe wave, it is almost possible to convert the band of about the 200 nm into the specific wavelength that we need.
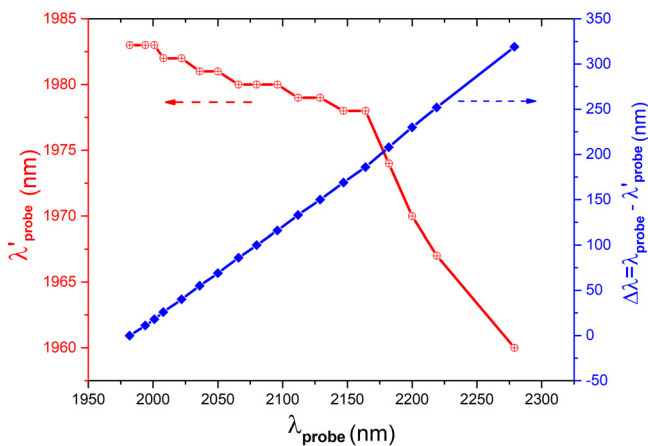

Fig. 4. Wavelength downward conversion diagram for different probe pulse wavelength. The wavelength of the pump pulse is located at $\lambda_{pump} = 2350$ nm. The λ_{probe} represents wavelength of the input probe pulse and it changes from 1980 nm to 2279 nm. The λ'_{probe} represents the probe pulse wavelength after wavelength conversion. The $\Delta\lambda$ represents the wavelength difference of the probe pulse wave before and after wavelength conversion.
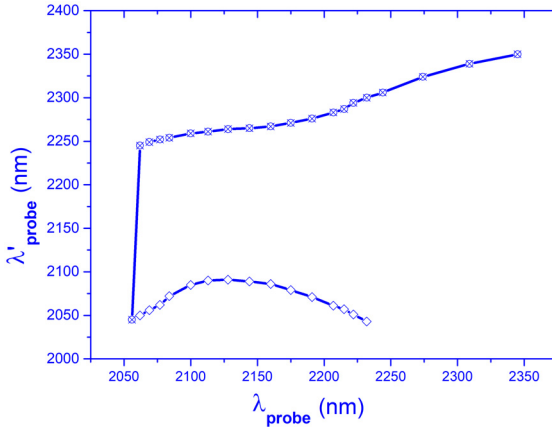
Fig. 5. Wavelength upward conversion diagram for different probe pulse wavelength. The wavelength of the pump pulse is located at λ_{pump} = 1550 nm. The λ_{probe} represents wavelength of the input probe pulse and it changes from 2056 to 2350 nm. λ'_{probe} represents the probe pulse wavelength after wavelength conversion.

The same mechanism can also be applied to long wavelength conversion, and the range of wavelength conversion is wider due to the group velocity matching curve. As it is shown in Fig. 5, when the probe wavelength is 2060 nm, a conversion of wavelength to long wavelength is generated. We can find not only the expected conversion of probe pulse to a new longer pulse, but also the conversion of part of low energy pulse to a new shorter pulse. This can be explained by four-wave mixing. As the position of the probe pulse moves towards the long wavelength on the premise of satisfying the group velocity matching, we can find that, when the probe pulse is between 2062 and 2232 nm, the new longer pulse and the new shorter pulse are always present here. In addition, we detected the energy of them, and found that the energy of the new longer pulse gradually decreased while that of the new shorter pulse continuously increased with the probe pulse wavelength moving from 2062 to 2232 nm. As the wavelength increases and beyond 2235 nm, one can only see that the new longer one produces a smaller frequency shift. This indicates that there is exchangeable wavelength conversion at the long wavelength side in the selected arsenic sulfide fiber. Like the short-wavelength conversion mechanism, the wavelength conversion is also produced under the premise of the collision of two pulses, which also shows that the ideal wavelength can be obtained by carefully controlling the fiber and pulse parameters.

4.2. The influence of probe pulse power

Next, we explore the relationship of wavelength conversion by changing the energy of the probe pulse wave. We only change the peak power of the pulse, everything else is the same. In this case, when exploring the conversion of power to long wavelength, we mainly mark the position of the high energy pulse after the transfer, while ignoring the very low energy pulse (it has no effect on the experimental results).
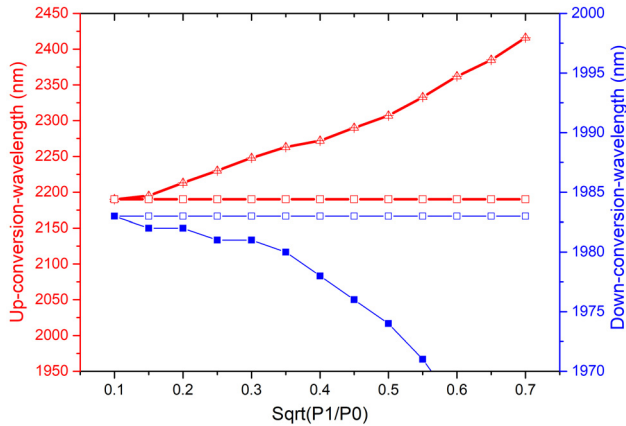
Fig. 6. Wavelength conversion diagram for different probe pulse power. The *x* axis of the graph represents the ratio of the peak power of the probe pulse to the pump pulse, which changes from 0.1 to 0.7. The blue lines represent a shift to longer wavelength. The probe pulse is located at λ_{probe} = 1983 nm, and the pump pulse is located at λ_{pump} = 1550 nm. The red lines represent a shift to shorter wavelength. The probe pulse is located at λ_{probe} = 2190 nm and the pump pulse is located at λ_{pump} = 2350 nm. In both cases all other parameters remain the same.

In Fig.6, the pump wave is located at 2350 nm and the probe pulse is located at 1983 nm; the power of probe pulse is changed from 150 to 750 W, equivalent to 0.01 times pump wave energy to 0.49 times pump wave energy. When we change the power of the probe pulse, one obvious change is that, the maximum wavelength of wavelength shift becomes significantly larger and it is changed from 1983 to 1963 nm. Previously, it was difficult to extend the supercontinuum at short wavelength due to the slope of the group velocity dispersion curve at short wavelength. This method shows that the wavelength can be extended to a shorter wavelength by increasing the power of the probe pulse, providing an effective way to extend the short wavelength of the supercontinuum spectrum. At the same time, as shown in this picture, the emitting position of the longer-wavelength pulse can be greatly and linearly changed by changing the power at the long-wavelength side, which also provides an effective way for us to broaden the wavelength to the mid-infrared.

5. Conclusion

In this work, longer wavelength and shorter wavelength than probe pulse wavelength are obtained by pumping two different pulses in the As_2S_3 fiber. The arsenic sulfide optical fiber has one zero dispersion wavelength (ZDW) and the input two pulses are set with a suitable time delay. It has been demonstrated that under the condition of group velocity matching, the collision location of probe pulse and pump wave can be precisely controlled by regulating the time delay, so as to accurately control the wavelength conversion. We also explore the influence of changing the position and the energy of the probe pulse; it not only realizes the frequency shift of the probe pulse, but

also realizes initial compression of pulse width. We find that increasing the power has a significant effect on the improvement of wavelength up conversion and wavelength down conversion, which is of great guidance for extending supercontinuum to shorter wavelength and even ultraviolet regions.

References

[1] CHENG T., NAGASAKA K., TUAN T.H., XUE X., MATSUMOTO M., TEZUKA H., SUZUKI T., OHISHI Y., *Mid-infrared supercontinuum generation spanning 2.0 to 15.1 μm in a chalcogenide step-index fiber*, Optics Letters **41**(9), 2016: 2117-2120. https://doi.org/10.1364/OL.41.002117

[2] SCHLIESSER A., PICQUÉ N., HÄNSCH T.W., *Mid-infrared frequency combs*, Nature Photonics **6**(7), 2012: 440-449. https://doi.org/10.1038/nphoton.2012.142

[3] DEMIRCAN A., AMIRANASHVILI S., STEINMEYER G., *Controlling light by light with an optical event horizon*, Physical Review Letters **106**(16), 2011: 163901. https://doi.org/10.1103/PhysRevLett.106.163901

[4] DENG Z., LIU J., HUANG X., ZHAO C., WANG X., *Active control of adiabatic soliton fission by external dispersive wave at optical event horizon*, Optics Express **25**(23), 2017: 28556-28566. https://doi.org/10.1364/OE.25.028556

[5] DUDLEY J.M., GENTY G., COEN S., *Supercontinuum generation in photonic crystal fiber*, Reviews of Modern Physics **78**(4), 2006: 1135-1184. https://doi.org/10.1103/RevModPhys.78.1135

[6] EL-AMRAOUI M., FATOME J., JULES J.C., KIBLER B., GADRET G., FORTIER C., SMEKTALA F., SKRIPATCHEV I., POLACCHINI C.F., MESSADDEQ Y., TROLES J., BRILLAND L., SZPULAK M., RENVERSEZ G., *Strong infrared spectral broadening in low-loss As-S chalcogenide suspended core microstructured optical fibers*, Optics Express **18**(5), 2010: 4547-4556. https://doi.org/10.1364/OE.18.004547

[7] GOUVEIA-NETO A.S., FALDON M.E., TAYLOR J.R., *Solitons in the region of the minimum group-velocity dispersion of single-mode optical fibers*, Optics Letters **13**(9), 1988: 770-772. https://doi.org/10.1364/OL.13.000770

[8] GU J., GUO H., WANG S., ZENG X., *Probe-controlled soliton frequency shift in the regime of optical event horizon*, Optics Express **23**(17), 2015: 22285-22290. https://doi.org/10.1364/OE.23.022285

[9] HUANG Y., YANG H., ZHAO S., MAO Y., CHEN S., *Design of photonic crystal fibers with flat dispersion and three zero dispersion wavelengths for coherent supercontinuum generation in both normal and anomalous regions*, Results in Physics **23**, 2021: 104033. https://doi.org/10.1016/j.rinp.2021.104033

[10] MISHRA V., SINGH S.P., HALDAR R., MONDAL P., VARSHNEY S.K., *Intermodal nonlinear effects mediated optical event horizon in short-length multimode fiber*, Physical Review A **96**(1), 2017: 013807. https://doi.org/10.1103/PhysRevA.96.013807

[11] PARK K., NA J., KIM J., JEONG Y., *Numerical study on supercontinuum generation in an active highly nonlinear photonic crystal fiber with anomalous dispersion*, IEEE Journal of Quantum Electronics **56**(2), 2020: 6800109. https://doi.org/10.1109/JQE.2020.2974519

[12] PETERSEN C.R., ENGELSHOLM R.D., MARKOS C., BRILLAND L., CAILLAUD C., TROLÈS J., BANG O., *Increased mid-infrared supercontinuum bandwidth and average power by tapering large-mode-area chalcogenide photonic crystal fibers*, Optics Express **25**(13), 2017: 15336-15348. https://doi.org/10.1364/OE.25.015336

[13] ROSENBERG Y., *Optical analogues of black-hole horizons*, Philosophical Transactions of the Royal Society A **378**(2177), 2020: 20190232. https://doi.org/10.1098/rsta.2019.0232

[14] ROBICHAUD L.R., FORTIN V., GAUTHIER J.C., CHÂTIGNY S., COUILLARD J.-F., DELAROSBIL J.-L., VALLÉE R., BERNIER M., *Compact 3–8 µm supercontinuum generation in a low-loss As$_2$Se$_3$ step-index fiber*, Optics Letters **41**(20), 2016: 4605-4608. https://doi.org/10.1364/OL.41.004605

[15] RONG J., MA Y., XU M., YANG H., *Interactions of the second-order solitons with an external probe pulse in the optical event horizon*, Chinese Optics Letters **20**(11), 2022: 111901. https://doi.org/10.1364/COL.20.111901

[16] RONG J., YANG H., XIAO Y., CHEN Y., *Mutual manipulation between a dark soliton and a probe wave for the gray-dark solitonic well*, Physical Review A **103**(2), 2021: 023505. https://doi.org/10.1103/PhysRevA.103.023505

[17] ROTHENBERG J.E., *Colliding visible picosecond pulses in optical fibers*, Optics Letters **15**(8), 1990: 443-444. https://doi.org/10.1364/OL.15.000443

[18] SKRYABIN D.V., GORBACH A.V., *Colloquium: Looking at a soliton through the prism of optical supercontinuum*, Reviews of Modern Physics **82**(2), 2010: 1287. https://doi.org/10.1103/RevModPhys.82.1287

[19] SUKHOIVANOV I.A., IAKUSHEV S.O., SHULIKA O.V., SILVESTRE E., ANDRÉS M.V., *Design of all-normal dispersion microstructured optical fiber on silica platform for generation of pulse-preserving supercontinuum under excitation at 1550 nm*, Journal of Lightwave Technology **35**(17), 2017: 3772-3779.

[20] THÉBERGE F., BÉRUBÉ N., POULAIN S., COZIC S., CHÂTIGNY S., ROBICHAUD L.-R., PLEAU L.-P., BERNIER M., VALLÉE R., *Infrared supercontinuum generated in concatenated InF$_3$ and As$_2$Se$_3$ fibers*, Optics Express **26**(11), 2018: 13952-13960. https://doi.org/10.1364/OE.26.013952

[21] WEBB K.E., ERKINTALO M., XU Y., BRODERICK N.G.R., DUDLEY J.M., GENTY G., MURDOCH S.G., *Nonlinear optics of fibre event horizons*, Nature Communications **5**(1), 2014: 4969. https://doi.org/10.1038/ncomms5969

[22] XIA C., KUMAR M., CHENG M.-Y., HEGDE R.S., ISLAM M.N., GALVANAUSKAS A., WINFUL H.G., TERRY F.L., FREEMAN M.J., POULAIN M., MAZÉ G., *Power scalable mid-infrared supercontinuum generation in ZBLAN fluoride fibers with up to 1.3 watts time-averaged power*, Optics Express **15**(3), 2007: 865-871. https://doi.org/10.1364/OE.15.000865

[23] YANG H., CHEN S., ZHAO S., YANG Y., *Observation of the quasi-discrete supercontinuum at optical event horizon*, Optics Communications **478**, 2021: 126379. https://doi.org/10.1016/j.optcom.2020.126379

[24] YU Y., ZHANG B., GAI X., ZHAI C., QI S., GUO W., YANG Z., WANG R., CHOI D.-Y., MADDEN S., LUTHER-DAVIES B., *1.8-10 µm mid-infrared supercontinuum generated in a step-index chalcogenide fiber using low peak pump power*, Optics Letters **40**(6), 2015: 1081-1084. https://doi.org/10.1364/OL.40.001081

[25] YULIN A.V., SKRYABIN D.V., RUSSELL P.S.J., *Four-wave mixing of linear waves and solitons in fibers with higher-order dispersion*, Optics Letters **29**(20), 2004: 2411-2413. https://doi.org/10.1364/OL.29.002411